UC Riverside
UC Riverside Previously Published Works

Title

The oxidation-reduction and electrocatalytic properties of CO dehydrogenase from Oligotropha carboxidovorans.

Permalink

https://escholarship.org/uc/item/5df7h538

Journal

Biochimica et biophysica acta. Bioenergetics, 1861(1)

ISSN

0005-2728

Authors

Kalimuthu, Palraj
Petitgenet, Mélanie
Niks, Dimitri
et al.

Publication Date

2020

DOI

10.1016/j.bbabio.2019.148118

Peer reviewed

ORIGINAL PAPER

Deconvolution of reduction potentials of formate dehydrogenase from *Cupriavidus necator*

Lindsey M. Walker[1] · Bin Li[1,2] · Dimitri Niks[3] · Russ Hille[3] · Sean J. Elliott[1]

Abstract

The formate dehydrogenase enzyme from *Cupriavidus necator* (FdsABG) carries out the two-electron oxidation of formate to CO_2, but is also capable of reducing CO_2 back to formate, a potential biofuel. FdsABG is a heterotrimeric enzyme that performs this transformation using nine redox-active cofactors: a bis(molybdopterin guanine dinucleotide) (bis-MGD) at the active site coupled to seven iron–sulfur clusters, and one equivalent of flavin mononucleotide (FMN). To better understand the pathway of electron flow in FdsABG, the reduction potentials of the various cofactors were examined through direct electrochemistry. Given the redundancy of cofactors, a truncated form of the FdsA subunit was developed that possesses only the bis-MGD active site and a singular [4Fe–4S] cluster. Electrochemical characterization of FdsABG compared to truncated FdsA shows that the measured reduction potentials are remarkably similar despite the truncation with two observable features at -265 mV and -455 mV vs SHE, indicating that the voltammetry of the truncated enzyme is representative of the reduction potentials of the intact heterotrimer. By producing truncated FdsA without the necessary maturation factors required for bis-MGD insertion, a form of the truncated FdsA that possesses only the [4Fe–4S] was produced, which gives a single voltammetric feature at -525 mV, allowing the contributions of the molybdenum cofactor to be associated with the observed feature at -265 mV. This method allowed for the deconvolution of reduction potentials for an enzyme with highly complex cofactor content to know more about the thermodynamic landscape of catalysis.

Keywords Formate dehydrogenase · Bis(molybdopterin guanine dinucleotide) · Protein film electrochemistry · Reduction potential

Introduction

As global CO_2 levels continue to rise, wreaking irreversible havoc on the environment and human health, a method to not only sequester CO_2 but also convert it into a clean fuel is becoming increasingly urgent [1]. Aside from the most commonly known method for CO_2 sequestration, the Calvin–Benson–Bassham cycle, autotrophic microbes are capable of using CO_2 as an energy source, thus sequestering it in the process [1]. Formate dehydrogenases (FDH) catalyze the reduction of CO_2 to formate, a feasible biofuel [2]. The FDH from the soil bacterium *Cupriavidus necator* (*Cn*) is cytosolic, has a molybdenum-based active site, and is dependent on NAD^+, thus giving it the advantage of being oxygen tolerant in contrast to most other metal-dependent FDHs [3]. *Cn* FDH carries out the two-electron oxidation of formate to CO_2 with NAD^+ serving as the electron acceptor; however, the enzyme has also been shown to be capable of the activation and reduction of CO_2 (Scheme 1), thus catalyzing both formate oxidation ($k_{cat} = 201$ s^{-1}) [4] and CO_2 reduction ($k_{cat} = 11 \pm 0.4$ s^{-1}) [5].

Cn FDH is encoded in the *fdsGBACD* operon which includes the genes for the subunits of the heterotrimeric enzyme, FdsABG, as well as maturation factors [6, 7]. Of the three subunits, FdsA is the largest (105 kDa) and contains
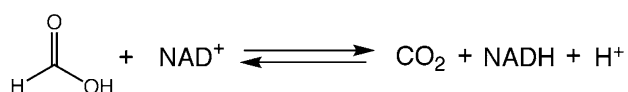
✉ Sean J. Elliott
elliott@bu.edu

1 Department of Chemistry, Boston University, 590 Commonwealth Avenue, Boston, MA 02215, USA

2 Department of Chemistry, University of Michigan, Ann Arbor, MI 48109, USA

3 Department of Biochemistry, University of California Riverside, 900 University Avenue, Riverside, CA 92521, USA

Scheme 1 Formate dehydrogenase reaction scheme

the bis-molybdopterin guanine dinucleotide cofactor (bis-MGD) active site similar to that found in other enzymes of the dimethyl sulfoxide (DMSO) reductase family; the metal coordination sphere is completed by a cysteine and terminal Mo=S ligand in a trigonal prismatic coordination geometry. In addition to the active site bis-MGD, the FdsA subunit has four [4Fe–4S] clusters and one [2Fe–2S] cluster. While FdsABG is yet to be crystallized, extensive modeling of the heterotrimer, based on the crystal structures of the formate dehydrogenase FdhF from *E. coli* and the homologous Nqo1, Nqo2 and Nqo3 subunits of the NADH dehydrogenase from *Thermus thermophilus,* predicts that electrons move from the FdsA subunit to FdsB via the series of iron–sulfur clusters, and through the FMN of FdsB, eventually reducing NAD^{+} [3]. The FdsG subunit (19 kDa) contains an additional [2Fe–2S] cluster, and the FdsB subunit (55 kDa) has an additional [4Fe–4S] cluster along with its FMN (Fig. 1a) [6]. The other two proteins encoded by this operon are FdsC and FdsD. FdsC bears a high similarity to the FdhD sulfurase from *E. coli* which receives a sulfur from IscS with which it sulfurates the molybdenum center prior to insertion into apoprotein [8]. FdsD shows no specific sequence similarity to any known enzyme, but due to its high surface charge (pI 9.9) it is thought to possibly play a role in shielding the cofactor from charge during transfer to the active site or in maintaining structural stability [6]. Previous work with the formate dehydrogenase from *R. capsulatus* clearly shows that both FdsC and FdsD must be present during protein maturation to result in an active enzyme that is fully loaded with Fe and the bis-MGD [7].

In total, FdsABG comprises nine cofactors, all of which are presumed to be redox active, providing for a complicated problem in terms of assigning specific reduction potentials and understanding the thermodynamics of electron transfer. Thus, in an effort to study the enzyme more effectively with respect to its redox-active cofactors and how electrons

flow in soluble FDHs, a simplified variant of the enzyme was constructed containing the minimal number of cofactors associated with the catalysis to occur: the molybdenum cofactor and a single [4Fe–4S] cluster (Fig. 1b). This truncated FdsA form, containing only the C-terminal portion of the subunit beginning at Ser235, reduces the size of the subunit from 105 to 82 kDa. The truncated FdsA is akin to the formate dehydrogenase from *E. coli,* FdhF, which similarly contains a singular [4Fe–4S] cluster and the active site molybdenum cofactor. With this truncated form of FdsA, we have been able to address the electrochemical characteristics of the active site as well as the associated [4Fe–4S] cluster.

Experimental section

Cloning of truncated FdsA, FdsC, and FdsD

The gene that encodes the full-length FdsA from *Cupriavidus necator* H16 (locus tag: H16_RS03175) was codon optimized for *E. coli* and synthesized in a pUC57 vector by Genscript, with an additional 3′-sequence for a C-terminal Strep-tag II (WSHPQFEK). To overexpress a minimal functional unit of FdsA, a plasmid that encodes an N-terminal truncated FdsA containing the binding motifs for a single [4Fe–4S] cluster and the molybdenum center was constructed. The coding region starting from Ser235 of the full-length FdsA was amplified by PCR using primers (Supporting information, Table 1), with 5′-SacII and 3′-HindIII restriction enzyme cut sites. The PCR product was digested by SacII and HindIII and inserted into the corresponding cloning sites of the pASK-IBA3 + vector, having ampicillin resistance, by T4 DNA ligase. The coding region of the plasmid was confirmed by sequencing (Genewiz). This construct maintained the C-terminal Strep-tag II for affinity purification. The truncated *fdsA* gene was then cloned into the pASK-IBA-3C vector (IBA Lifesciences) to have chloramphenicol resistance using the restriction enzymes HindIII HF and XbaI, followed by ligation with T4 DNA ligase.

Additionally, the *fdsC* and *fdsD* genes from *Cupriavidus necator* H16 (locus tag: H16_RS03180 and H16_RS03185) were codon optimized and synthesized in a pUC57 vector by

Fig. 1 **a** Cartoon of the heterotrimeric formate dehydrogenase (FdsABG) from *C. necator* showing the various cofactors. **b** Cartoon of the truncated FdsA produced
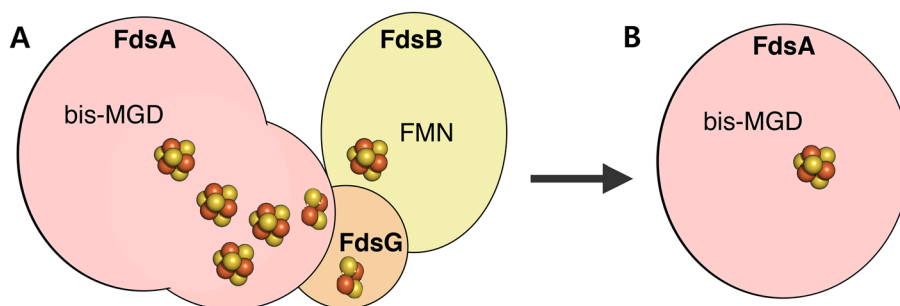
Table 1 Specific activity and metal content analysis of formate dehydrogenase constructs

	Specific activity (Units/mg)	Mo content (atoms/monomer)	Fe content (atoms/monomer)
FdsABG	70	–	–
Truncated FdsA with Mo cofactor	8.5	N.D.	4
Truncated FdsA without Mo cofactor	0.02	0	5

Genscript. The two genes were subcloned to the MCS1 of pETDuet-1 vector to form a di-cistronic *fdsCD* in two steps. First, the *fdsC* and *fdsD* genes were amplified by PCR with a 5′-NcoI and 3′-SpeI and BamHI sites, using primers CF/CR and DF/DR, respectively (Table S2). The PCR products were digested by NcoI and BamHI, and, after purification through electrophoresis and gel extraction (Qiagen), were inserted to the corresponding sites of pETDuet-1 by T4 DNA ligase, to generate two separate plasmids fdsC_pETDuet-1 and fdsD_pETDuet-1. Second, fdsC_pETDuet-1 was digested by SpeI and BamHI and fdsD_pETDuet-1 was digested by XbaI (a restriction site from the pETDuet-1 vector) and BamHI, respectively. The large fragment from fdsC_pETDuet-1 (~6.2 kb) and the small fragment from fdsD_pETDuet-1 (~0.3 kb) were purified and ligated by T4 DNA ligase at the compatible ends generated at SpeI/XbaI site and the BamHI site. The resultant plasmid contains both *fdsC* and *fdsD* genes under the same T7 promoter, each with a ribosomal binding site (AAGGAG). All primers were synthesized by Life Technologies. All plasmid sequences were confirmed by sequencing (Genewiz).

Growth and expression

The pASK-3C vector containing the truncated Fd*sA* gene was co-transformed with the pETDuet vector containing the *fdsC* and *fdsD* genes into the *E. coli* BL21(DE3) ΔiscR cell line [9] and then plated on LB-agar with 100 μg/mL ampicillin and 35 μg/mL chloramphenicol (GoldBio). After overnight growth at 37 °C, a single colony was selected to inoculate a 5 mL starter culture of 2xYT with the same antibiotics and then grown overnight at 37 °C and 180 rpm. The 5 mL starter culture was diluted into 1 L of 2xYT and grown at 37 °C and 200 rpm until it reached an O.D. of about 0.8. The cells were cooled at 4 °C for 30 min prior to inducing the pASK-IBA3C plasmid with 0.2 μg/mL anhydrotetracycline (Sigma-Aldrich) and the pETDuet-1 plasmid with a final concentration of 100 μM IPTG (GoldBio) and supplementing the media for cofactor

loading with 0.2 mM sodium molybdate and 0.25 mM ammonium ferrous sulfate (Sigma-Aldrich) before growing overnight at 24 °C and 100 rpm for protein maturation. Cells were harvested by centrifugation about 14 h after induction and pellets were stored at −20 °C prior to protein purification. Growth conditions are based on those performed previously for the formate dehydrogenases from *R. capsulatus* and *C. necator* [4, 7].

To isolate the truncated FdsA protein without the molybdenum center, the pETDuet-1 plasmid was omitted from the transformation process described above. Consequently, ampicillin was also omitted from the media. The cells were only induced with anhydrotetracycline and no sodium molybdate was added to the media so as to ensure that the molybdenum center would not be matured. All other conditions were kept constant across growth and expression for the truncated FdsA with and without the molybdenum center.

Purification of Fds constructs

Truncated FdsA was purified by employing the Strep-tag located at the C-terminal of the enzyme. The cell pellet collected from 1 L of media was resuspended in 30 mL of buffer A and supplemented with 1 mg/mL lysozyme, DNase, and 1 mM phenylmethylsulfonyl fluoride (PMSF). Buffer A comprised 100 mM monosodium phosphate, 10 mM nitrate to stabilize the molybdenum cofactor, and 5% (w/v) glycerol, all at pH 7.2. The suspension was chilled on cold beads for 10 min prior to lysing the cells via sonication with a Branson 450 Sonifier with six rounds of 10 s with a 20% output and 40% duty cycle with about 30 s of rest in between cycles. Clarified lysate was collected via centrifugation at $15000g$ for 35 min at 4 °C. The clarified lysate was loaded on to a 10 mL Strep-Tactin Sepharose (IBA Lifesciences) column pre-equilibrated with buffer A. The column was washed with five column volumes of buffer A before eluting with three column volumes of buffer A supplemented with 2.5 mM *d*-desthiobiotin. The elution was concentrated with an Amicon Centrifugal Filter with a molecular weight cut off of 50 kDa to about 1 mL and stored immediately in liquid nitrogen. Truncated FdsA was confirmed for purity with a 12% SDS-PAGE gel.

The truncated FdsA lacking the mature molybdenum center was purified in the same manner described above with the only exception being that buffer A contained no sodium nitrate. All steps of the purifications were performed anaerobically in a Coy Lab anaerobic chamber with an atmosphere of 3% hydrogen balanced with nitrogen.

FdsABG was grown and purified in the manner described previously [4].

Activity measurements

Specific activity measurements were performed on the FdsABG, truncated FdsA with no Mo, and truncated FdsA with Mo. Measurements were made at 30 °C in a 75 mM potassium phosphate buffer at pH 7.2, 40 mM formate substrate, and 100 mM benzyl viologen to act as the electron acceptor, and concentrations of the protein ranged from 20 nM to 5 μM. Change in the absorbance of the benzyl viologen at 600 nm was measured for 10 s upon addition of formate and specific activity is reported in Units/mg. Protein concentration for specific activity measurements was determined via Bradford colorimetric assay (Bio-Rad). All steps of activity measurements were performed anaerobically in a sealed quartz cuvette (Starna), degassed with Ar, and kept under an Ar atmosphere. Protocol for activity measurements was based on previous work by Friedebold et al. [10].

Determination of metal content

Iron content was determined for truncated FdsA with and without Mo via colorimetric Fe assays as well as inductively coupled plasma emission spectroscopy (ICP-ES). Mo content was determined via ICP-ES. A colorimetric iron assay was performed according to the procedure previously described [11]. An iron standard curve was constructed from a 100 μg/mL stock solution with concentrations ranging from 0 to 2 μg/mL. The protein sample was reduced with 0.02% ascorbic acid dissolved in 0.2 M HCl and allowed to sit at room temperature for 5 min before precipitating the protein with 0.5 mL of 11.3% trichloroacetic acid. The precipitated protein was removed via centrifugation at 10,000g for 5 min after which 1 mL of supernatant was transferred to a fresh microcentrifuge tube and 0.4 mL 10% ammonium acetate was added followed by 0.1 mL of the ferroin color reagent which was made by dissolving 75 mg of ferrozine and 75 mg neocuproine in 25 mL milliQ H_2O with one drop of concentrated hydrochloric acid. Absorbance measurements were taken in quintuplicate at 561 nm. A standard curve was constructed from the solutions of known Fe concentration and a line of best fit was identified from which the unknown Fe concentrations for the protein samples were determined.

Inductively coupled plasma emission spectrometry (ICP-ES) was performed to identify the stoichiometry of both Fe and Mo in the truncated FdsA. The enzyme was tested for Mn, Fe, Zn, and Mo by preparing a 40 mL stock solution of 25 ppm for each metal in 1% nitric acid. A standard curve for each metal was prepared with concentrations of 0.1, 0.25, 0.5, 1, 5, and 10 ppm. The truncated FdsA was acidified in 1% nitric acid for 10 min prior to centrifugation at 10,000g for 5 min to remove the protein precipitant. A standard curve was determined for each metal with known concentrations

and was fit to an equation of a line from which the concentration of the metal in the FdsA sample was determined. Each point was subtracted from background absorbance and was measured in duplicate. The ICP-ES experiments were performed on a Jobin-Yvon Ultima-C ICP-ES.

Electrochemical measurements

Electrochemical experiments were performed with a PGSTAT 12 potentiostat (EcoChemie) under anaerobic conditions in a MBraun Labmaster glovebox under a nitrogen atmosphere. A three-electrode configuration was used where the reference electrode was a standard calomel electrode (SCE) (Accumet) and the counter electrode was a platinum wire. The temperature of the cell was controlled by a water jacket, maintaining a temperature of 4 °C or 10 °C. All potentials are reported relative to a standard hydrogen electrode which was calibrated quarterly against the $Fe(CN)_6^{3-}/Fe(CN)_6^{4-}$ redox couple at 20 °C and pH 7.0.

All experiments were performed using a pyrolytic graphite edge (PGE) electrode that had been pretreated by mechanical polishing on 120 grit and 1500 grit sandpaper followed by incubating overnight at room temperature with 20 μL of 3 mg of multi-walled carbon nanotubes (MWCNT) (Sigma, 10 nm ± 1 nm × 4.5 nm ± 0.5 nm × 3–6 μm) dissolved in 1 mL of dimethylformamide (DMF) by sonication for 15 min [12]. All experiments were performed using a mixed buffer solution 10 mM (MES, CHES, HEPES, CAPS, and TAPS), 200 mM NaCl, and pH 7.5.

Determination of reduction potentials

Baseline cyclic voltammograms (CV) were measured over a potential range starting at − 0.2 V to − 1 V vs SCE for three full cycles at either 4 °C or 10 °C with scan rates of 10, 50, 100, and 200 mV/s. Baseline square wave voltammograms were measured starting at − 1 V to − 0.2 V vs SCE with an amplitude of 50 mV and frequencies of 10 or 15 Hz at either 4 °C or 10 °C; these low temperatures were found to be necessary to form a stable protein film, as the film appeared to desorb at 25 °C and 30 °C after a few minutes. The protein film of either FdsABG (80 μM), truncated FdsA with Mo (94 μM), or truncated FdsA without Mo (150 μM) was generated by directly depositing 4 μL of protein on to the PGE electrode surface modified with MWCNT and allowing the solution to sit at room temperature for about 3 min before gently rinsing with buffer and depositing electrodes into the electrochemical cell containing pre-equilibrated buffer. This method had been successfully used previously to increase current outputs specifically for enzymes with buried, redox-active [4Fe–4S] clusters and hydrogenase enzymes [13–15]. Both truncated FdsA and FdsABG protein films were generated

on unmodified PGE electrodes, both by directly depositing the protein on the electrode surface in the presence or absence of the co-adsorbant polymyxin (1 mg/mL). However, the use of MWCNT was found to be essential to generate consistent and stable signals above the background capacitance. This method for generating a protein film for all three enzyme constructs resulted in stable and reproducible voltammetry for over 30 min and over at least three different protein films. Identical conditions for the cyclic and square wave voltammograms were used with the protein film present, as used for the baseline. Non-turnover electrochemical signals were analyzed by correction of the non-Faradaic component of the current from the raw data using the QSoas package [16].

Electrocatalytic experiments were carried out in a similar manner with FdsABG. Baseline measurements of the PGE electrode modified with MWCNT were measured at 10 °C, a scan rate of 2 mV/s, and rotation rate of 1000 rpm, all in the same mixed component buffer at pH 7.5. The FdsABG enzyme film was generated at the electrode surface in the same manner described for the non-turnover experiments. A CV was measured under the same conditions as baseline prior to adding formate to the electrochemical cell. Formate was added in excess to the electrochemical cell with a final concentration of 5 mM and CVs were measured under the same conditions described for the baseline measurements to ensure the resulting current was coming as a direct result of FdsABG oxidation of formate.

Results

Purification and characterization of truncated FdsA

SDS-PAGE was used to assess the quality of the purification of truncated FdsA, both with and without the molybdenum center present. During a typical purification, the cell pellet from a 2 L growth yielded ~ 3 mg of truncated FdsA, with a significant amount of the enzyme lost in the flow-through and washing step over the Strep-Tactin column as revealed by the by SDS-PAGE and visually through the loss of the deep brown color on the column. However, the SDS-PAGE gel revealed a single band of pure protein at the expected molecular weight of 80 kDa for protein, either containing or missing the molybdenum center (Fig. 2a, b), demonstrating that the truncated FdsA can be successfully purified in the absence or presence of the molybdenum center.

Omission of the *fdsC and fdsD* genes required for maturation of the molybdenum cofactor allowed for truncated FdsA to be prepared without the active site cofactor, therefore having no ability to carry out formate oxidation, but still retaining a singular [4Fe–4S] cluster. Analysis of the bis-MGD-free truncated FdsA by optical absorption revealed an absorbance at 420 nm, as expected for the presence of an oxidized [4Fe–4S] cluster (Fig. 3a). The Fe content per truncated FdsA monomer was quantified by a colorimetric ferrozine assay which showed a stoichiometric ratio of four atoms Fe to one protein monomer. These results were corroborated by ICP-ES experiments, which showed five
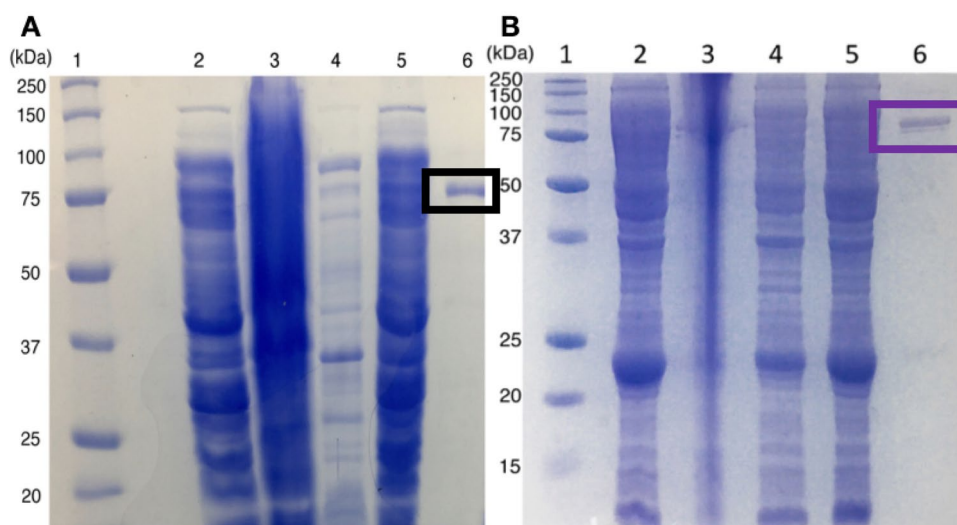

Fig. 2 Purified truncated FdsA visualized by SDS-PAGE. **a** SDS-PAGE for the purification of truncated FdsA with the bis-MGD cofactor mature and **b** without the bis-MGD cofactor with the ladder of proteins of known molecular weight (lane 1), the solubilized fraction (lane 2), the insoluble fraction (lane 3), the flow-through from the Strep-Tactin column (lane 4), the wash off the Strep-Tactin column (lane 5), and the concentrated elution off the column (lane 6). The final concentrated truncated FdsA is boxed (black, purple) with the molecular weight just above the ladder marker at 75 kDa
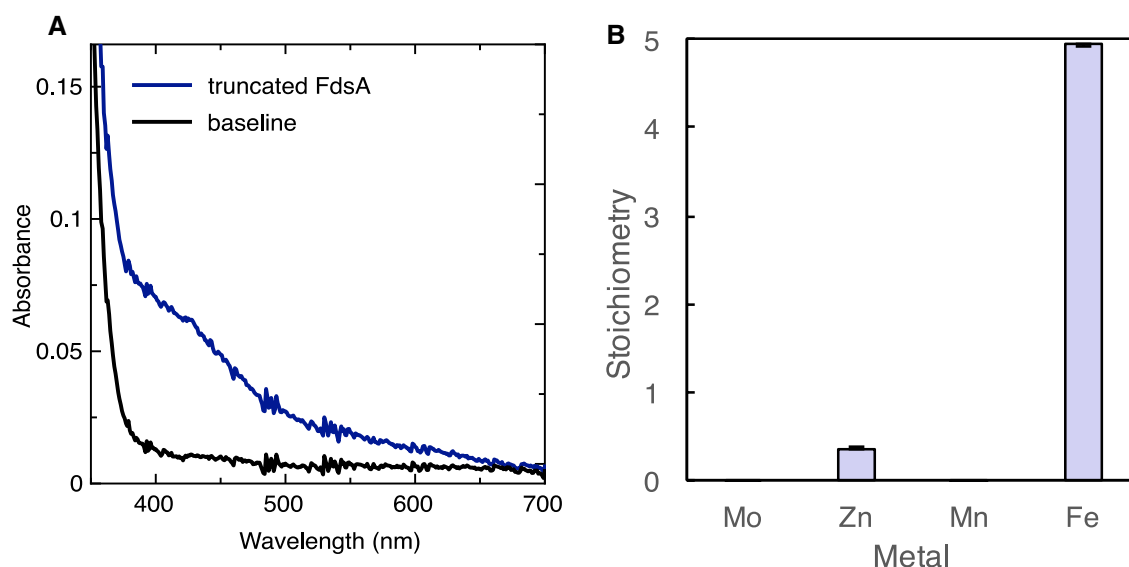
Fig. 3 Characterization of metal cofactors in truncated FdsA. **a** UV–visible spectrum of truncated FdsA without bis-MGD bound (blue) compared to baseline (black). **b** Graph of the stoichiometric ratio between metal centers (Mo, Zn, Mn, and Fe) for the bis-MGD-free version of truncated FdsA as determined by ICP-ES

atoms Fe per protein monomer and no Mo was present in the enzyme (Fig. 3b) when the concentration of the protein was determined by Bradford assay. The slightly higher than expected stoichiometry between Fe and FdsA could result from adventitiously bound Fe or the inherent $\pm 20\%$ error in determining the protein concentration via Bradford assay. Lastly, the complete lack of Mo in this 'apo' truncated FdsA shows that when the chaperones FdsC and FdsD are absent during protein expression, the molybdenum cofactor cannot be matured and delivered, as was previously observed in the case of the FDH from *R. capsulatus* [7]. As the 'apo' truncated FdsA is missing the mature molybdenum cofactor, the enzyme is essentially inactive, showing a specific activity of 0.02 unit/mg. On the other hand, when FdsA is co-expressed with FdsC and FdsD, the truncated FdsA shows significantly greater activity with 8.5 Units/mg. While this is about ten times less than that achieved with the natively purified, full-length heterotrimeric FdsABG (70 Units/mg) [4], it is significantly greater than the enzyme that has no detectable Mo present, fully consistent with the role of FdsC and FdsD in maturation and incorporation of the molybdenum center. The results of the metal content analysis and specific activity data are summarized in Table 1.

Identification of reduction potentials for truncated FdsA and FdsABG

The electrochemical methods of cyclic voltammetry (CV) and square wave voltammetry (SWV) were used to characterize the reduction potentials of the various redox-active cofactors in both the native, heterotrimeric FdsABG from the native organism (Fig. 4a, b) and the truncated FdsA with or without the molybdenum cofactor (Fig. 4C and 4D). The CV of full-length FdsABG revealed a broad envelope that included averaged maxima at -410 mV and -265 mV vs SHE. Likewise, the reduction potentials determined by SWV were -420 mV and -260 mV vs SHE (Fig. 4a, b). As discussed below, these data must indicate the electrochemical response of the dominant FMN, as well as the molybdenum and iron–sulfur centers. The CV of truncated FdsA, bearing the singular [4Fe–4S] cluster and molybdenum center, was much better resolved, showing two distinct features (Fig. 4c) at -265 mV and -455 mV vs SHE; SWV data yielded similar reduction potentials of -450 mV and -260 mV vs SHE (Fig. 4d). Between the full-length heterotrimer FdsABG and the truncated FdsA, the resulting reduction potentials are remarkably similar. Importantly, the FdsABG data show a highly intense peak with a full-width-at-half-height (FWHH) of about 70 mV. The reduction potential of this feature, as well as its sharpness, and pH dependence (Figure S1) of this feature likely indicate flavin that has been directly adsorbed to the graphite electrode. Yet, the overall envelope suggests the contribution of several individual one-electron redox couples (Fig. 4a), making it impossible to assess individual redox couples FdsABG as a whole. In contrast, the truncated FdsA data are much simpler: there are just two specific couples of note, where by CV the higher-potential feature has an FWHH of about 130 mV, not showing the sense of cooperativity as observed in case of FdsABG and indicating the absence of the FMN housed in the FdsB subunit.

The catalytic response of FdsABG was assessed to ensure its activity on the electrode surface (Fig. 5). However, the

Fig. 4 Voltammetry of truncated FdsA and FdsABG. Cyclic voltammetry of FdsABG (**a**) (red) and truncated FdsA (**c**) (blue) and with baselines (black) measured at 10 °C, pH 7.5, and scan rates of 50 mV/s. **b** Square wave voltammograms FdsABG (red) and **d** truncated FdsA (blue) measured at 10 °C, pH 7.5, and a frequency of 10 Hz and 15 Hz, respectively
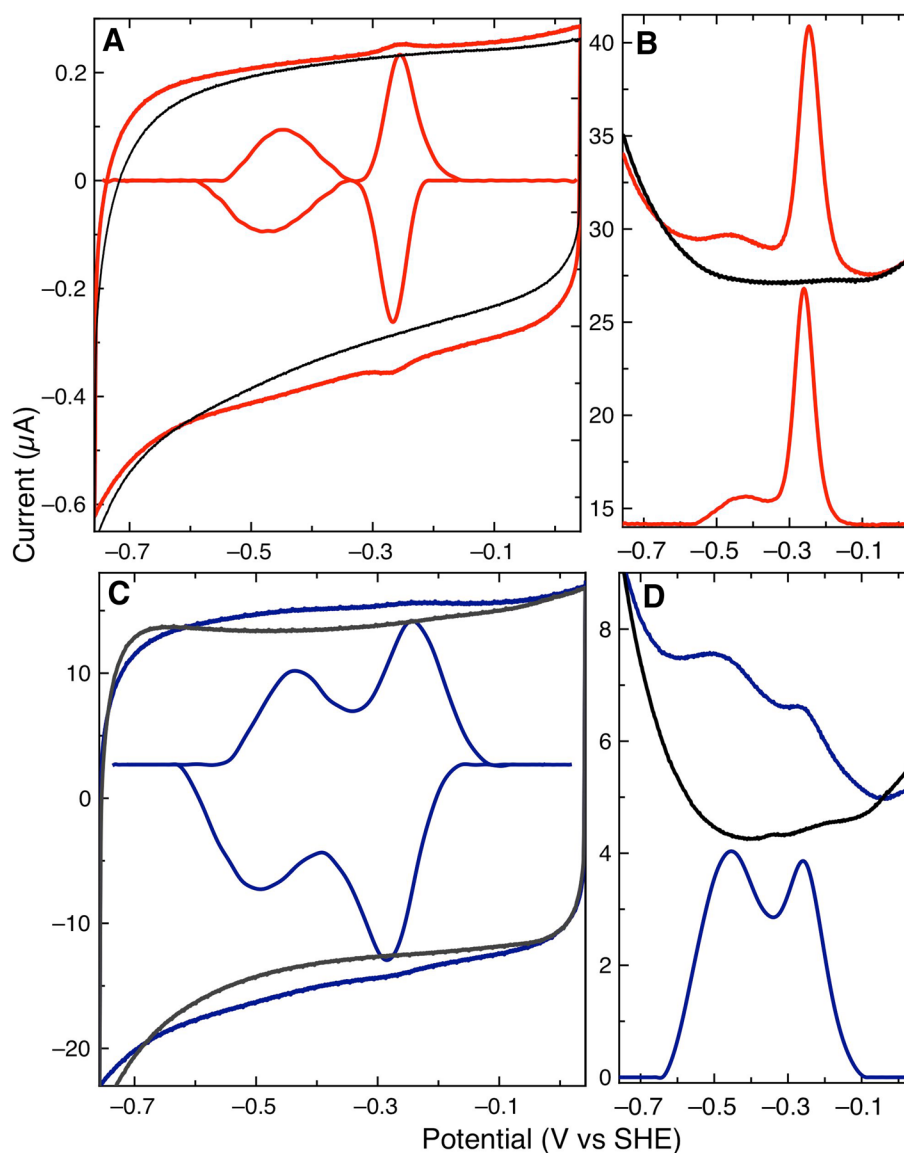
conditions used to for the electrocatalysis were not optimal for maximizing turnover: a low temperature (10 °C) was shown to be required for protein film stability. When formate was present in excess in the electrochemical cell, a clear oxidative current associated with formate oxidation was observed for FdsABG (Fig. 5, blue trace). While the current output observed for FdsABG is less than what has previously been observed by Hirst and co-workers for the formate dehydrogenase enzymes from *E. coli* and *Syntrophobacter fumaroxidans*, these results nonetheless show that FdsABG is active and also shows that the formate oxidation begins to occur near − 400 mV just like other formate dehydrogenases previously studied via electrocatalytic methods [17, 18]. This result suggests that FdsABG operates via the same mechanism for formate oxidation as the FDHs from *E. coli* and *Syntrophobacter fumaroxidans*. The truncated construct of FdsA was not electrocatalytically active, however, likely

due to the low-temperature conditions required for film stability and the decreased activity of FdsA in comparison to FdsABG. As seen above, truncated FdsA was found to be tenfold less active that the full-length enzyme in solution-based activity measurements, suggesting that the possible electrocatlytic activity of truncated FdsA is buried in the noise of these experiments.

To interrogate the nature of the oxidation–reduction couples observed in truncated FdsA and to assign these couples, truncated FdsA was expressed and purified in a fashion that would yield an enzyme that was devoid of the molybdenum-containing cofactor. The protein was thus prepared by omitting the necessary *fdsC* and *fdsD* genes associated with maturation from the expression system. The resulting protein, lacking the molybdenum cofactor, was characterized in the same manner as described for both the 'holo' truncated FdsA, with the bis-MGD and FeS cluster, and FdsABG.
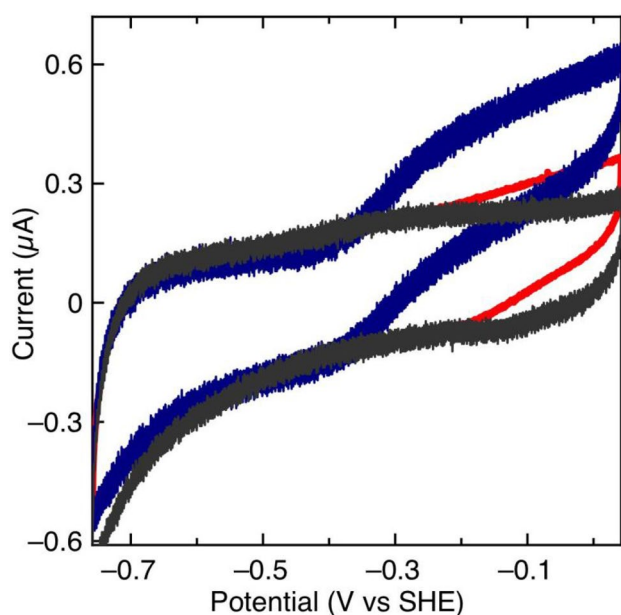
Fig. 5 Electrocatalytic turnover of formate by FdsABG. Cyclic voltammetry of FdsABG measured at 10 °C, pH 7.5, a scan rate of 2 mV/s and electrode rotation rate of 1000 rpm in the presence (blue) and absence (red) of 5 mM formate measured against the bare electrode (gray) under the same conditions

Both CV and SWV revealed a singular feature centered at −525 mV vs SHE (Fig. 6a, b); by CV this couple was clearly quasi-reversible with a slightly greater current generated in the reductive wave and a more broadened current in the oxidative wave. Further interrogation of this couple by altering the scan rate did not modulate the appearance of the data. Given the lack of the bis-MGD cofactor in this construct and the presence of the [4Fe–4S] cluster as determined by
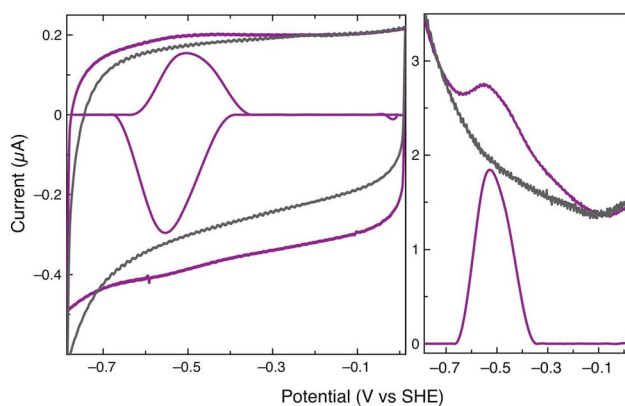

Fig. 6 Voltammetry of truncated FdsA purified without bis-MGD cofactor. Cyclic voltammetry (**a**) and square wave voltammetry (**b**) of truncated FdsA purified without the bis-MGD cofactor (purple) with baselines (black) measured at 4 °C, pH 7.5, with a scan rate of 50 mV/s and a frequency of 15 Hz respectively

elemental analysis, we can attribute this electrochemical data to the [4Fe–4S]$^{2+/1+}$ redox couple.

Apparent reduction potentials determined for each of the three enzyme forms examined here determined by CV are summarized in Table 2. In general, the full-length and truncated forms of the enzymes are surprisingly similar despite the loss of seven redox-active cofactors. The reduction potential measured for the truncated FdsA without bis-MGD present permits assignment of the observed potential to the single [4Fe–4S] cluster present, albeit at a somewhat higher potential than seen in the absence of the molybdenum center. The additional higher-potential feature observed with truncated FdsA with the molybdenum cofactor present was to be assigned to this site by a process of elimination. The higher-potential feature in the FdsABG CV is proposed to also belong to the FMN cofactor given its peak current and narrower FWHH of 70 mV, indicative of a two-electron transfer process. However, because this feature is clearly present also in truncated FdsA which has no FMN present, it is proposed that the feature observed at −262 mV in the FdsABG CV comprised reduction potentials for both the FMN and Mo cofactor. The similarity in reduction potentials between presumed FMN and the Mo cofactor suggests that the flavin-based redox reactions of the FdsABG enzyme are similar in potential to the FdsA active site.

Discussion

The formate dehydrogenase from *Cupriavidus necator* is a complex enzyme, where the large number of redox-active cofactors complicates conventional attempts to resolve reduction potentials by direct electrochemistry or spectroscopically driven assays. Indeed, our original goal of deconvoluting the individual cofactor reduction potentials proved impossible here. Desorption of flavin at the carbon electrodes used and the possibility of overlap of multiple signals (Fig. 4a) illustrate just how hard problems such as these are in the world of protein electrochemistry. However, here we developed a strategy for resolving the potentials of individual cofactors by simplifying the enzyme, to the absolute minimum number of cofactors necessary for enzyme activity: the bis-MGD and the proximal [4Fe–4S] cluster. We

Table 2 Reduction potentials of various constructs of formate dehydrogenase from *C. necator*

Protein	E_1 (mV vs SHE)	E_2 (mV vs SHE)
FdsABG	−460	−262
Truncated FdsA	−455	−265
Truncated FdsA without bis-MGD	−525	–

confirm that the FdsC and FdsD chaperones are essential for maturation and insertion of the bis-MGD cofactor into FdsA, as had been shown previously with the formate dehydrogenase from *R. capsulatus* [7]. The residual activity of truncated FdsA prepared in the absence of co-expressed FdsC and FdsD, is likely due to a small amount of cofactor incorporation using the maturation machinery endogenous to *E. coli* [7, 19]). Co-expression with FdsC and FdsD along with supplementation with molybdenum results in an increase in activity from essentially no activity to tenfold less than the full-length enzyme. While conditions for cofactor maturation can perhaps be further optimized, it is likely that the activity of the truncated enzyme is intrinsically lower than that of the heterotrimer given the missing cofactors and the possible coupling that occurs between the native redox partner and formate. Meanwhile, the formate oxidation activity achieved from the truncated FdsA shows that this enzyme does in fact have the minimum cofactors required to carry out the two-electron oxidation of formate, providing us with a model system for examining the reduction potentials of the FdsA active site and proximal [4Fe–4S] cluster.

From the electrochemical analysis of the truncated FdsA, two distinct features are observed, suggesting one can be attributed to the molybdenum cofactor and the other to the [4Fe–4S] cluster. Given that maturation of the molybdenum center depends upon the co-expression of FdsC and FdsD, we have been able to prepare truncated FdsA lacking the molybdenum cofactor, making it possible to unambiguously assign the low reduction potential to the [4Fe–4S] cluster. Our results clearly show that the higher-potential feature seen with replete truncated FdsA is missing when the molybdenum cofactor is absent; thus, we can assign this potential (-265 mV) to the molybdenum center; the lower potential feature (-455 mV) can then be assigned to the $[4Fe–4S]^{2+/1+}$ redox couple of the most proximal FeS cluster. We note that the potential of this feature in truncated FdsA (with or without cofactor) is similar to a feature found in the holo FdsABG enzyme, suggesting that the most proximal cluster has the (nearly) same potential in the holo complex. Likewise, given that the feature at -265 mV clearly vanishes in the absence of the molybdenum cofactor, the reduction potential can be ascribed to this cofactor by a process of elimination. With that, the exact nature of the features (i.e., the precise Mo(IV/V) and Mo(V/VI) one-electron redox couples) remains eluvise. Assigning the molecular nature of the feature observed at -265 mV is a challenge by direct electrochemistry alone, though it is clear that the broad nature of the feature in truncated FdsA precludes considering the feature to be a cooperative, two-electron Mo(IV/VI) couple. Previously, various Mo and pyranopterin features have been reported for other bis-MGD bearing enzymes: For example, the Mo-containing enzyme YedY has been proposed to have reduction potentials at -239 mV and -261 mV coming from a pyranopterin dihydro-tetrahydro interconversion, while the Mo (V/IV) couple is proposed to have a potential of $+174$ mV [20]. Additionally, the Mo-containing enzyme SorT showed reduction potentials of 110 mV and -18 mV for the Mo(VI/V) and Mo(V/IV) redox, respectively, from solution-based experiments [21]. The molybdopterin-containing enzyme NarGHI has been reported to have reduction potentials of 190 mV and 95 mV assigned to the Mo(V/VI) and Mo(IV/V) redox couples, respectively [22, 23]. Here, the apparent Mo-based redox events in our system are much higher in potential than those of the formal formate/CO_2 redox couple [18], and are ~60 mV more positive than of benzyl viologen (though our assays were conducted at very high formate concentrations). Together, these observations suggest that the system is biased toward formate oxidation, versus CO_2 reduction. Yet, we realize that in our truncated FdsA, the absence of the N-terminal domain likely modulates the Mo(IV/V), (V/VI) redox couples. Thus, we conclude that our system will provide the opportunity to probe the features that contribute to the control of the Mo-based active site, but until then we can only ascribe the redox properties of the Mo cofactor generally.

Looking at further studies to assess the holo FdsABG enzyme in greater detail, challenges abound. Here, our strategy has been to arrive at a minimal enzymatic unit to try and simplify FdsA to the point of comparisons with the *E. coli* enzyme, or other formate dehydrogenases. Removal of the N-terminus, and the two other components of the homotrimeric holoenzyme, has allowed us to evaluate the redox chemistry of the proximal [4Fe–4S] cluster. The broad part at the lower potential feature seen with the full-length enzyme does suggest that one or more cofactors are close enough together in reduction potential that they appear as a singular broad feature, most likely due to some undefined subset of the seven remaining FeS clusters in the FdsABG. We find that the cluster remaining in the truncated FdsA is similar in reduction potential to the low-potential features of the holoenzyme, but removal of the molybdopterin active site (by producing the enzyme without FdsC and FdsD) results in a negative shift in reduction potential of ~70 mV (deletion of the molybdenum center in NarGHI results in a similarly large decrease in potential [22]). Further assessing individual FeS clusters will likely require the development of new Fds constructs. Meanwhile in the higher-potential regime, the sharpness of the electrochemistry in holoenzyme has implicated flavin dissociation, where non-specific two-electron non-specific redox chemistry [24] is observed, as opposed to two separate one-electron transfers [25–27] that would have a stoichiometry associated with the iron–sulfur clusters and molybdopterin, as would be ideal. This dilemma is a continued challenge to probing the direct electrochemistry of many complex enzymes where flavin-based domains

associated with interconversions of the NAD(P)H pool are coupled to enzymatic subunits, such as FdsA.

Conclusions

Investigating truncated FdsA alongside the full-length FdsABG has provided greater insight into the electrochemistry of the system. The truncated FdsA prepared and examined here is identical in cofactor constitution to FdhF from *E. coli*, supporting the hypothesis that only the successfully matured molybdenum center and one [4Fe–4S] cluster are in fact necessary to achieve formate oxidation, although the remaining cofactors are certainly required for electron transfer on to NAD$^+$. The ability to manipulate the system to include (or not) the molybdenum center has allowed us to unambiguously assign the reduction potentials of the [4Fe–4S] cluster and the molybdenum center to be assigned to -455 mV and -265 mV vs SHE, respectively, which provides insight into how electrons flow upon formate oxidation. Through our simplification and electrochemical study of the *C. necator* formate dehydrogenase, this FDH can now be better contextualized within its enzyme family and provide information on its energy landscape.

References

1. Solomon S, Plattner G-K, Knutti R, Friedlingstein P (2009) Proc Natl Acad Sci USA 106:1704
2. Müller J, MacEachran D, Burd H, Sathitsuksanoh N, Bi C, Yeh Y-C, Lee TS, Hillson NJ, Chhabra SR, Singer SW, Beller HR (2013) Appl Environ Microbiol 79:4433
3. Hille R, Hall J, Basu P (2014) Chem Rev 114:3963–4038
4. Niks D, Duvvuru J, Escalona M, Hille R (2016) J Biol Chem 291:1162–1174
5. Yu X, Niks D, Mulchandani A, Hille R (2017) J Biol Chem 292:16872–16879
6. Oh J-I, Bowien B (1998) J Biol Chem 273:26349–26360
7. Hartmann T, Leimkühler S (2013) FEBS J 280:6083–6096
8. Thomé R, Gust A, Toci R, Mendel R, Bittner F, Magalon A, Walburger A (2012) J Biol Chem 287:4671–4678
9. Akhtar MK, Jones PR (2008) Appl Microbiol Biotechnol 78:853–862
10. Friedebold J, Mayer F, Bill E, Trautwein AX, Bowien B (1995) Biol Chem Hoppe-Seyler 376:561–568
11. Carter P (1971) Anal Biochem 40:450–458
12. McDowall JS, Murphy BJ, Haumann M, Palmer T, Armstrong FA, Sargent F (2014) Proc Natl Acad Sci 111:E3948–E3956
13. Ayikpoe R, Ngendahimana T, Langton M, Bonitatibus S, Walker LM, Eaton SS, Eaton GR, Pandelia M-E, Elliott SJ, Latham JA (2019) Biochemistry 58:940–950. https://doi.org/10.1021/acs.biochem.8b01082
14. Walker LM, Kincannon WM, Bandarian V, Elliott SJ (2018) Biochemistry 57:6050–6053
15. McDowall JS, Murphy BJ, Haumann M, Palmer T, Armstrong FA, Sargent F (2014) Proc Natl Acad Sci USA 111:E3948
16. Fourmond V (2016) Anal Chem 88:5050–5052
17. Bassegoda A, Madden C, Wakerley DW, Reisner E, Hirst J (2014) J Am Chem Soc 136:15473–15476
18. Reda T, Plugge CM, Abram NJ, Hirst J (2008) Proc Natl Acad Sci USA 105:10654
19. Schlindwein C, Giordano G, Santini CL, Mandrand MA (1990) J Bacteriol 172:6112–6121
20. Adamson H, Simonov AN, Kierzek M, Rothery RA, Weiner JH, Bond AM, Parkin A (2015) Proc Natl Acad Sci USA 112:14506
21. McGrath AP, Laming EL, Garcia GPC, Kvansakul M, Guss JM, Trewhella J, Calmes B, Bernhardt PV, Hanson GR, Kappler U, Maher MJ (2015) eLife 4:e09066
22. Rothery RA, Magalon A, Giordano G, Guigliarelli B, Blasco F, Weiner JH (1998) J Biol Chem 273:7462–7469
23. Wu S-Y, Rothery RA, Weiner JH (2015) J Biol Chem 290:25164–25173
24. Heering HA, Hagen WR (1996) J Electroanal Chem 404:249–260
25. Baymann F, Schoepp-Cothenet B, Duval S, Guiral M, Brugna M, Baffert C, Russell MJ, Nitschke W (2018) Frontiers in Microbiology 9:1357
26. Lim ZH, Chng ELK, Hui Y, Webster RD (2013) J Phys Chem B 117:2396–2402
27. Tan SLJ, Novianti ML, Webster RD (2015) J Phys Chem B 119:14053–14064